An artificial neural network-enhanced energy management strategy for plug-in hybrid electric vehicles

Shaobo Xie [a, 1], Xiaosong Hu [b, c, *, 1], Shanwei Qi [a], Kun Lang [a]

[a] School of Automotive Engineering, Chang'an University, Southern 2nd Road, Xi'an 710064, China
[b] State Key Laboratory of Mechanical Transmissions, Department of Automotive Engineering, Chongqing University, Chongqing 400044, China
[c] Advanced Vehicle Engineering Centre, Cranfield University, Cranfield, MK43 0AL, UK

ARTICLE INFO

Article history:
Received 6 May 2018
Received in revised form
15 July 2018
Accepted 20 August 2018
Available online 22 August 2018

Keywords:
Plug-in hybrid electric vehicle
Equivalent consumption minimum strategy
Equivalent factor
Artificial neural network
Pontryagin's minimum principle

ABSTRACT

In order to achieve near-optimal fuel economy for plug-in hybrid electric vehicles (PHEVs) using the equivalent consumption minimum strategy (ECMS), it is necessary to dynamically tune the equivalent factor (EF). Unlike widely used model-based approaches, this paper proposes a data-driven ECMS that determines the EF using an artificial neural network (ANN). First, by comparing Pontryagin's Minimum Principle (PMP) with the ECMS, one can find that the EF is related to the co-state value of the PMP method. Then, an ANN is constructed with three accessible input variables, including the current demanded power, the ratio of the distance travelled to the total distance, and the battery State of Charge (SOC). The neural network is subsequently trained using real-world speed profiles. Simulations are performed considering different initial SOC values. The results reveal that the proposed data-driven ECMS demonstrates satisfactory fuel economy compared to global optimization methods like dynamic programming and PMP methods. The computational time of the proposed method relative to the duration of the entire trip indicates a great potential for the development of a time-conscious energy management strategy. Moreover, the impact of training sample size on the ANN performance is discussed.

1. Introduction

In recent years, transportation electrification has been gaining growing attention worldwide for the sake of fuel economy improvements, greenhouse gas emission reductions, as well as less dependence on fossil fuels [1]. In particular, plug-in hybrid electric vehicles (PHEVs) have been increasingly investigated, as they address range anxiety and enable energy-source diversification via vehicle-grid interaction [2].

Integrating more than two power sources within a hybrid powertrain makes it necessary to carefully devise an energy management strategy (EMS), so as to coordinate power-flow distribution for better fuel economy. Various methods have been proposed to develop EMSs, including rule-based or fuzzy logic methods [3,4], optimization theory-based methods [5–7], and artificial intelligence methods [8,9].

Despite a common choice for commercial hybrids [3], rule-based EMSs, which depend on practical engineering experience, prevent them from being applied to make the most of hybrid powertrains. Fuzzy logic has been introduced to improve the flexibility of such rules [10]. However, a significant weakness of rule-based methods lies in the fact that they cannot realize optimal or near-optimal fuel economy due to a lack of optimality. Dynamic programming (DP) algorithms that can produce a provably globally optimal solution have been widely used. However, driving cycle information is required to be known *a priori*. Thus, real-time applications of DP algorithms cannot be easily achieved [11]. Stochastic DP algorithms have been suggested by considering the randomness of speed distribution [12,13]. Owing to massive iterative and interpolation calculations required to estimate the cost-to-go, the DP methodology is often time-consuming [14]. Nonetheless, it is often regarded as a benchmark to evaluate other EMSs, thanks to salient optimality. The Pontryagin's Minimum Principle (PMP) algorithm is another global optimization algorithm used to develop EMSs. It determines the optimal power-allocation policy by

* Corresponding author. State Key Laboratory of Mechanical Transmissions, Department of Automotive Engineering, Chongqing University, Chongqing 400044, China.
E-mail address: xiaosonghu@ieee.org (X. Hu).
[1] S. Xie and X. Hu equally contributed to this research work.

https://doi.org/10.1016/j.energy.2018.08.139
0360-5442/

Nomenclature

P_r	demanded power
P_{bat}	total battery power
P_b	power consumed by electrical load
P_l	battery internal power loss
P_m	total motor power
P_{egu}	EGU output power
P_{aux}	power consumed by auxiliary components
Q_b	battery capacity
U_{oc}	battery open circuit voltage
R_b	battery internal resistance
J	total cost
L	instantaneous cost
H	Hamilton function
m_f	fuel rate
c_f, c_e	prices of fuel fossil and electricity
$\frac{l}{L}$	ratio of travelled distance to total distance
λ	co-state variable
S	equivalent factor
E_b	battery energy

List of abbreviations

SOC	battery stage of charge
HEV	hybrid electric vehicle
PHEV	plug-in hybrid electric vehicle
EMS	energy management strategy
EGU	engine-generator-unit
DP	dynamic programming
PMP	Pontryagin's minimum principle
ECMS	equivalent consumption minimum strategy
EF	equivalent factor
MPC	model predictive control
ANN	artificial neural network
ANN-ECMS	artificial neural network based equivalent consumption minimum strategy

instantaneously minimizing the Hamiltonian function [15–17], thereby greatly reducing the computational burden. Similar to the DP method, the PMP method requires prior knowledge of driving cycle. However, both DP and PMP methods can be implemented over a moving horizon to capture a local optimal solution, yielding a model predictive control (MPC)-based EMS [18,19].

The equivalent consumption minimum strategy (ECMS) derived from the PMP algorithm makes a real-time EMS possible, which has become an alternative to develop EMSs [6]. The ECMS, which was originally applied to HEVs [20], provided that the consumed battery power was offset by the on-board engine, was then extended to PHEVs [21]. However, a key issue about implementing the ECMS still remains, that is, how may the equivalent factor (EF) - a critical scaling factor that determines the proportion of energy consumed from fuel and the battery- be dynamically tuned so as to accomplish energy consumption similar to that determined by a global optimization algorithm, e.g., DP. As such, various approaches to tuning the EF have been reported. For example, an adaptive ECMS (A-ECMS) calibrates the EF based on the feedback on the SOC deviation from a preset reference [22–24]. Thus, it is important for the A-ECMS to construct a reference SOC by leveraging the available information, e.g., the distance travelled or telematics information [25]. It is worth noting that the reference SOC for PHEVs and HEVs are totally different. Specifically, the reference SOC for the former varies with driving environment, i.e., the distance travelled, whereas the one for the latter can be set to a constant level (e.g. 0.6), due to charge sustenance over a trip [26]. Moreover, taking into account different energy conversion efficiencies during driving and braking of HEVs, two constants, rather than a single one, have been used to define the EF [5]. A map-based ECMS for PHEVs has been proposed as well, in which the optimal energy distribution is performed offline and stored in tables so that the EF can be determined by searching the tables online [22]. Furthermore, an improved adaptive equivalent consumption minimization strategy (IA-ECMS) has been designed to instantaneously adjust the EF based on the identified driving behavior and predicted real-time traffic information [27]. The particle swarm optimization algorithm has been put forward to tune the EF for a plug-in hybrid city bus in Ref. [28]. Fuzzy logic has also been utilized to calculate the EF [29].

Additionally, artificial neural networks have been exploited to develop EMSs. Generally, the selection of input and output variables for an artificial neural network significantly affects the network performance and its utilization/generalization. Eleven variables were chosen as network inputs to predict the demanded output [9]. In addition, two individual neural networks were deployed to develop an EMS, where the first network performed SOC planning, and the second network realized power distribution [30].

The aforementioned approaches to adjusting the EF in ECMSs of PHEVs can be viewed as model-based ECMSs. Within model-based ECMSs, e.g., techniques based on SOC deviation feedback control from a SOC reference, the SOC reference is established involving an initial SOC value. This means that the model-based controller intended for a specific SOC level may not be applicable to cases with other different initial SOC levels, greatly weakening the robustness of the controller. Actually, due to many uncertain conditions, initial SOC levels for PHEVs always alter in daily running and are thus unfixed. From this perspective, a data-driven method that has the potential of covering various initial SOC levels during neural network training could be favorable. As a result, to bridge this research gap, this paper proposes a data-driven artificial neural network-enhanced ECMS (ANN-ECMS). Main contributions have been made to distinguish our study from existing ones. First, a framework of an artificial neural network based ECMS is proposed, and a spectrum of cases with different initial SOC levels is utilized to examine the proposed method. Second, a concise neural network structure with three accessible input variables is established, with the aim of improving the computational efficiency and reducing the controller memory. Finally, the impact of training sample size on the ANN-ECMS performance is evaluated based on real-world driving cycles, and the time efficiency of ANN-ECMS is systematically contrasted to other typical methods. A significant advantage of the proposed method is the capability of dealing with changeable initial SOC levels and improving the robustness of the controller.

The remainder of this paper is organized as follows. Section 2 describes the powertrain model, and Section 3 establishes the relationship between the EF and co-state by equating the PMP algorithm to the ECMS. Then, the PMP algorithm is applied to real-world speed profiles to generate training data in Section 4. The proposed artificial neural network is detailed and trained in Section 5. After that, Section 6 presents the framework for the ANN-ECMS. Section 7 displays important results, followed by main conclusions in Section 8.

2. PHEV modeling

The PHEV examined in this study is based on a prototype in Ref. [31] and has a serial configuration, as illustrated in Fig. 1. An integrated-starter-generator (ISG) and a diesel engine are mechanically coupled to form an engine-generator-unit (EGU) that can supply electric energy to the battery. The electrical machine (EM), with the efficiency contour plot in Fig. 2, can operate as either a driving motor or a generator. The maximum generating power of the EM is limited to 30 kW during regenerative braking, taking into account the battery health. The specifications of powertrain are summarized in Table 1. By combining the brake specific fuel consumption (BSFC) of the engine and the generator efficiency, the equivalent energy efficiency of the EGU can be calculated, as plotted in Fig. 3, with the optimal EGU fuel rate indicated by the red line.

2.1. Battery model

An equivalent electrical circuit to simulate the lithium ion phosphate battery system is shown in Fig. 4. The open circuit voltage and equivalent internal resistance are functions of the battery SOC, neglecting the effects of temperature [32]. Based on experimental data, the estimated open circuit voltage and equivalent internal resistance of a battery cell are plotted in Fig. 5.

The power balance equation of the battery system is formulated as

$$P_{bat} = P_b + P_l = \quad P_b + I^2 R_b \tag{1}$$

where P_{bat} is the internal battery power, P_b is the terminal battery power, and P_l is the internal power loss of the battery; I is the electrical current, and R_b is the equivalent internal resistance.

According to (1), the battery dynamics can be described by

$$\dot{SOC} = f(SOC) = -\frac{U_{oc} - \sqrt{U_{oc}^2 - 4R_b P_b}}{2Q_b R_b} \tag{2}$$

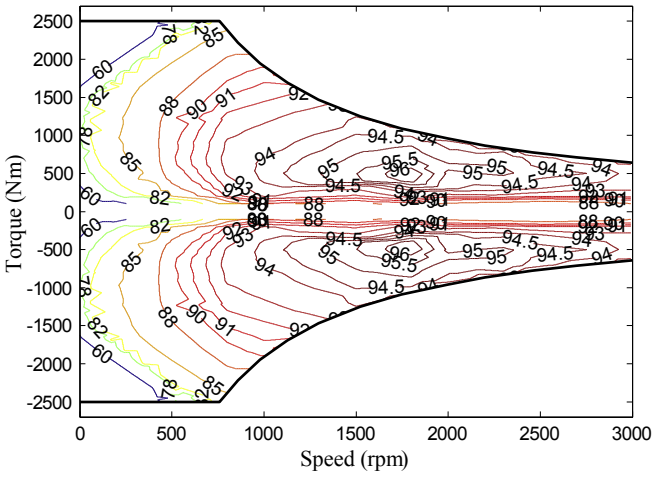

Fig. 2. Torque/Speed curve and Efficiency contour plot of electrical machine [31].

Table 1
Powertrain Parameters [31].

Item	Parameter	Value
Vehicle	Mass/kg	16500
	Final gear ratio	6.733
Electrical machine	Peak power/kW	150
	Peak torque/Nm	2100
	Peak speed/rpm	3000
ISG	Peak power/kW	90
	Peak torque/Nm	330
	Peak speed/rpm	3000
Engine	Displacement/L	2.78
	Peak power/kW	110
	Peak speed/rpm	3200
Battery	Voltage/V	537.6
	Capacity/Ah	180

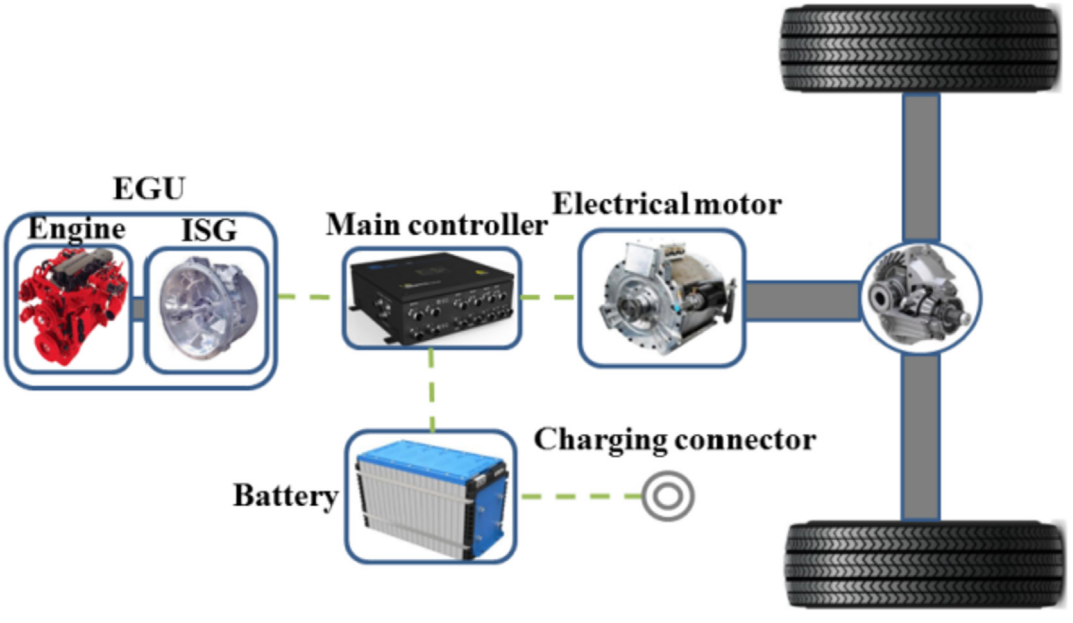

Fig. 1. Powertrain architecture in PHEV [31].

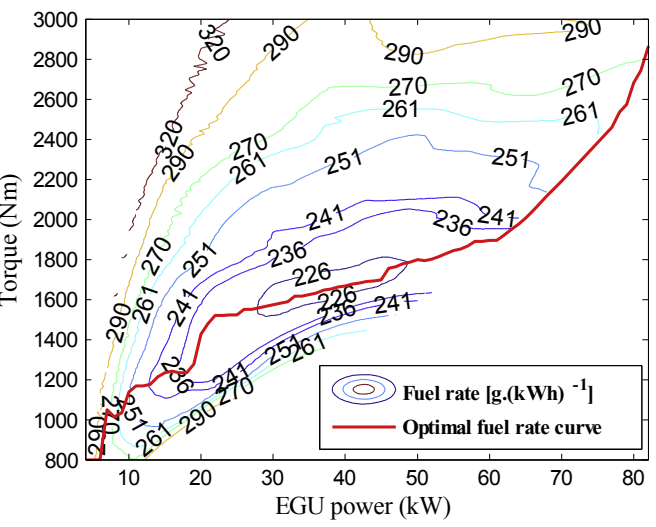

Fig. 3. Equivalent energy efficiency contour plot of EGU [31].

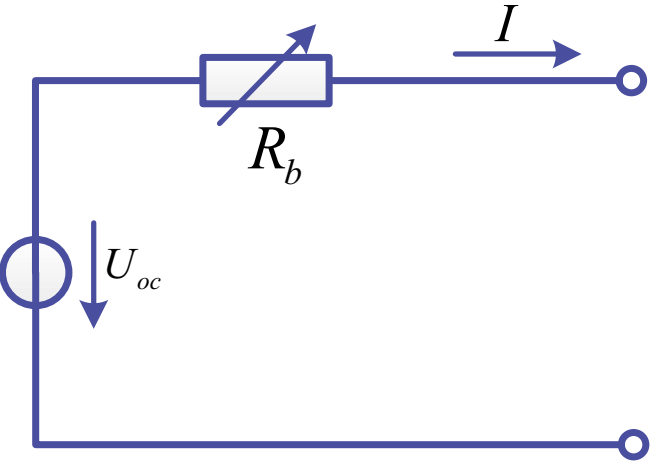

Fig. 4. Equivalent electric circuit of battery.

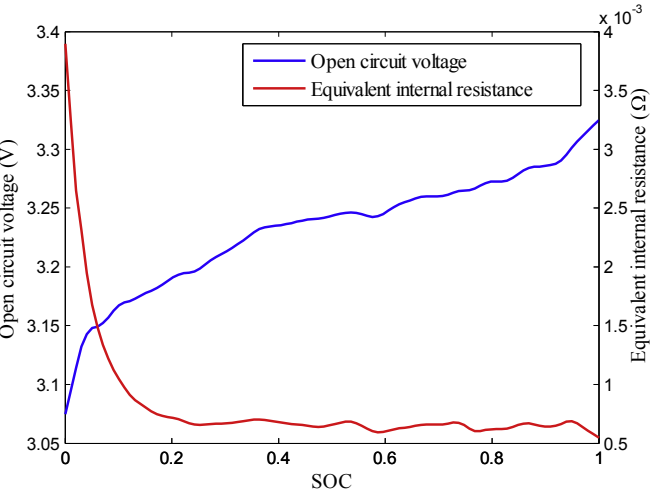

Fig. 5. Open circuit voltage and equivalent internal resistance of battery cell [14].

where Q_b is the nominal battery capacity, and U_{oc} is the open circuit voltage.

2.2. Vehicle dynamics

For the PHEV, the vehicle-level power balance equation can be formulated as follows:

$$\frac{1}{3600}\left(mgfv + \frac{C_d A}{21.15}v^3 + \xi m\frac{dv}{dt}v\right) = P_m \eta_m^{sgn(P_m)} \tag{3}$$

$$P_b + P_{egu} = P_m + P_{aux} \tag{4}$$

where m is the mass, f is the rolling resistance coefficient, C_d is the air resistance coefficient, A is the front area, v is the speed, ξ is the equivalent mass inertia, η_m is the electric efficiency of the motor, and P_m is the total power consumed by the motor or the recuperated power during braking. When P_m is larger than zero (for propelling), sgn equals 1; when P_m is less than zero (for recuperation), sgn equals -1. Moreover, P_{egu} is the EGU output power, and P_{aux} is the power consumed by auxiliary components, e.g., the electrical steering system and the braking system.

3. Relationship between PMP and ECMS

As the ECMS can be essentially derived from the PMP method, the two methods can be tied, as shown in the following.

3.1. PMP

The PMP minimizes the total cost of energy consumption over a trip, including the fuel cost and electricity cost, which has the form of [15,17]:

$$J = min\int_0^{t_f} L(\cdot)dt = min\int_0^{t_f}\left(c_f\dot{m}_f + c_e\frac{P_{bat}}{3600}\right)dt \tag{5}$$

where J denotes the total cost; L is the instantaneous cost; t_f is the trip duration; c_f and c_e are the unit prices for fuel (CNY.L^{-1}) and electricity (CNY.kWh^{-1}), respectively; $\dot{m}_f$ is the fuel rate (L.s^{-1}), and P_{bat} is the total battery power.

Consequently, the Hamiltonian function can be expressed as

$$H = c_f\dot{m}_f + c_e\frac{P_{bat}}{3600} + \lambda\dot{SOC} \tag{6}$$

where λ is the co-state variable, which is governed by the co-state dynamics:

$$\dot{\lambda} = -\frac{\partial H}{\partial SOC} = -\lambda\frac{\partial\dot{SOC}}{SOC}. \tag{7}$$

And the normal equation is described as

$$\dot{SOC} = \frac{\partial H}{\partial\lambda}. \tag{8}$$

When minimizing the Hamiltonian function, the SOC upper and lower boundary constraints should be satisfied:

$$\left\{SOC_{initial} = SOC_0,\ SOC_{end} = SOC_f\right\}.$$

Additionally, the physical limitations imposed on the power components are given below:

$$\begin{cases} P_{bat,min} \le P_{bat}(t) \le P_{bat,max}, \\ P_{egu,min} \le P_{egu}(t) \le P_{egu,max}, \\ T_{m,min} \le T_m(t) \le T_{m,max}, \\ n_{m,min} \le n_m(t) \le n_{m,max} \end{cases}.$$

3.2. ECMS

The ECMS instantaneously minimizes the equivalent energy consumption cost, with the objective function described as [22,33]:

$$J = c_f \dot{m}_f + S(t)\frac{c_e P_{bat}}{3600} \tag{9}$$

where $S(t)$ is the EF.

3.3. Relationship between both methods

The SOC dynamics can be rewritten as

$$\dot{SOC} = f(SOC) = -\frac{I}{Q} = -\frac{IU_{oc}}{QU_{oc}} = -\frac{P_{bat}}{3.6E_b} \tag{10}$$

where E_b denotes the battery energy, kJ.

Then the Hamiltonian function can be rewritten as

$$H = c_f \dot{m}_f + \frac{P_{bat}}{3600}\left(c_e - \frac{1000\lambda}{E_b}\right). \tag{11}$$

Comparing (6) and (11) yields

$$c_e - \frac{1000\lambda(t)}{E_b} = c_e S(t). \tag{12}$$

Then,

$$S(t) = 1 - \frac{1000\lambda(t)}{c_e E_b}. \tag{13}$$

Equation (13) demonstrates that the optimal EF, $S(t)$, of the ECMS can be determined, if the optimal co-state value, λ, of the PMP is known, similar to the conclusion in Ref. [34].

4. Acquisition of network training data

In this section, the PMP algorithm is employed to generate a data set for the neural network training in Section 5.

4.1. Samples of driving cycle

The bus route considered in Xi'an city, China has a round-trip distance of around 71 km, and the speed profiles along this route during a half-year period were acquired. As the bus route is almost flat, the road gradient was neglected. Without loss of generality, five speed profiles were randomly chosen from the data set for the neural network training and verification, as shown in Fig. 6. Specifically, the speed profiles (No.1 - No.4) were used for the network training, while the last one (No.5) for the network verification. In addition, to evaluate the impact of sample size on the network performance, two cases are considered: case 1 based on two speed profiles (No.1 - No.2) and case 2 based on four speed profiles (No.1 - No.4).

As the initial SOC levels for a PHEV vary from trip to trip due to many random factors, the initial SOCs for the network training change from 0.3 to 0.9 with an increment of 0.1; seven cases with different initial SOCs are hence considered for performing a comprehensive network training.

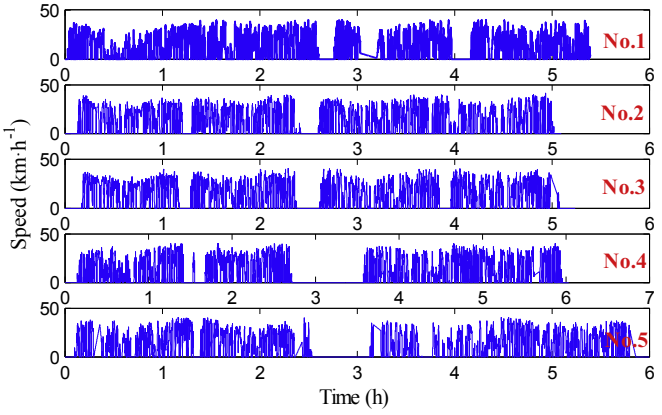

Fig. 6. Speed profiles along city bus route.

4.2. Solution of PMP

As the PMP algorithm often cannot be solved analytically, the shooting method is leveraged to obtain the mathematical solution, where the secant method is used to calibrate the initial co-state value in each shooting [17],

$$\begin{cases} \lambda_i = \lambda_0 \ (i = 1), \lambda_i = \lambda_{i-1} + \delta \ (i = 2), \lambda_i \\ \quad = \lambda_{i-1} - (\lambda_{i-1} - \lambda_{i-2})\dfrac{SOC_{i-1} - SOC_f}{SOC_{i-1} - SOC_{i-2}} \ (i = 3, 4, \cdots) \end{cases}. \tag{14}$$

where i is the shooting index; λ_i (i=1,2) are the first two initial co-state values determined by constants λ_0 and δ; SOC_f is the final SOC value, which is set to 0.3.

The detailed flowchart of the shooting method is presented in Fig. 7, where k is the time step, the parameter ε is used to control the shooting time and computational accuracy, which is specified as 0.001. Furthermore, the values of λ_0 and δ are set to −64.5 and 0.05, respectively, for all cases.

4.3. Results and analysis

To demonstrate the process of solving the PMP algorithm, a particular case, with an initial SOC of 0.9 and speed profile No.1, is presented. The SOC profiles generated by the shooting method are shown in Fig. 8. Six shootings are iterated before the algorithm converges, indicating that the final SOC in the sixth shooting can reach the preset scope. Also, it can be observed that the SOC profile experiences a gradual decline during the whole shooting process. Accordingly, six initial co-state values adjusted by the secant method in each shooting increased before reaching a stable level, as illustrated in Fig. 9. The optimal co-state trace, which is generated in the sixth shooting process, reveals the power distribution policy, as portrayed in Fig. 10.

The optimal co-state traces for case 1 (No.1 and No. 2 speed profiles as training samples) and case 2 (No.1 to No. 4 speed profiles as training samples) with seven different initial SOCs are shown in Figs. 11 (a) and Fig. 12 (a). Two optimal co-state traces and four optimal co-state traces are yielded, respectively, for case 1 and case 2, under different initial SOC levels. It can be seen that the co-state traces move downward as the initial SOC reduces from 0.9 to 0.3.

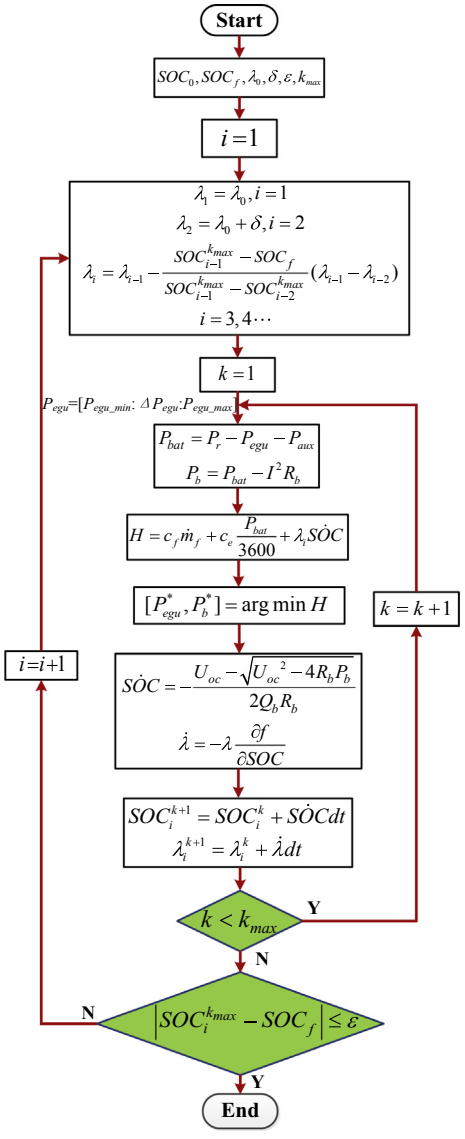

Fig. 7. Flowchart of shooting method.

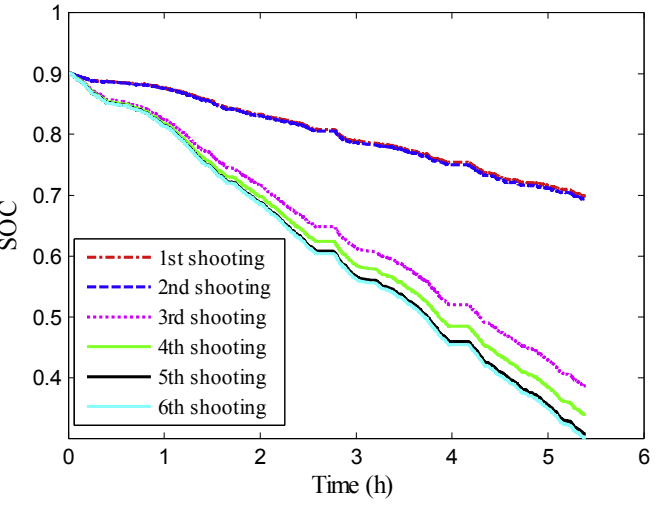

Fig. 8. SOC profiles during shooting method.

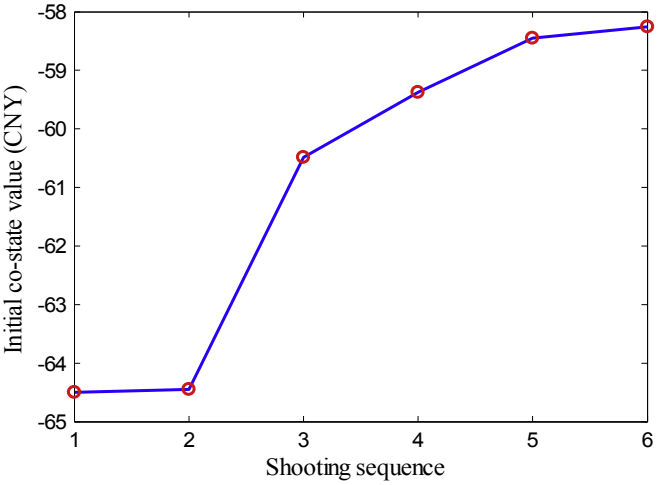

Fig. 9. Initial co-state values during shooting method.

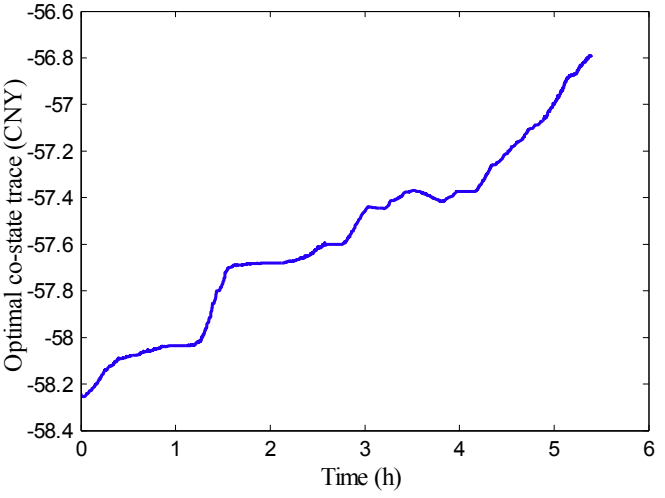

Fig. 10. Optimal co-state trace.

Also, it is notable that almost all co-state traces maintain a rising tendency over the trip, except the case of the initial SOC of 0.3, as shown in Figs. 11 (b) and Fig. 12 (b). When the initial SOC is 0.3, the SOC is maintained by a charging-sustaining state, leading to a declining co-state trace, whereas in all the other cases, the SOC declines over the trip, leading to rising co-state traces.

5. Neural network modeling

5.1. Neural network structure

A common three-layer back-propagation neural network is adopted, as illustrated in Fig. 13. Three variables are chosen as network inputs: the current demanded power P_r, the battery SOC, and the ratio of the distance travelled to the total distance $\frac{l}{L}$.

The demanded power P_r is computed by

$$\left\{ P_r(k) = \frac{1}{3600}\left(mgfv(k) + \frac{C_d A}{21.15} v(k)^3 + \delta m \frac{\Delta v(k)}{\Delta t} v(k) \right), \frac{\Delta v(k)}{\Delta t} = \frac{v(k) - v(k-1)}{3.6\Delta t} \right\} \tag{15}$$

where $\frac{\Delta v(k)}{\Delta t}$ is the acceleration at the k-th time step, and Δt is the

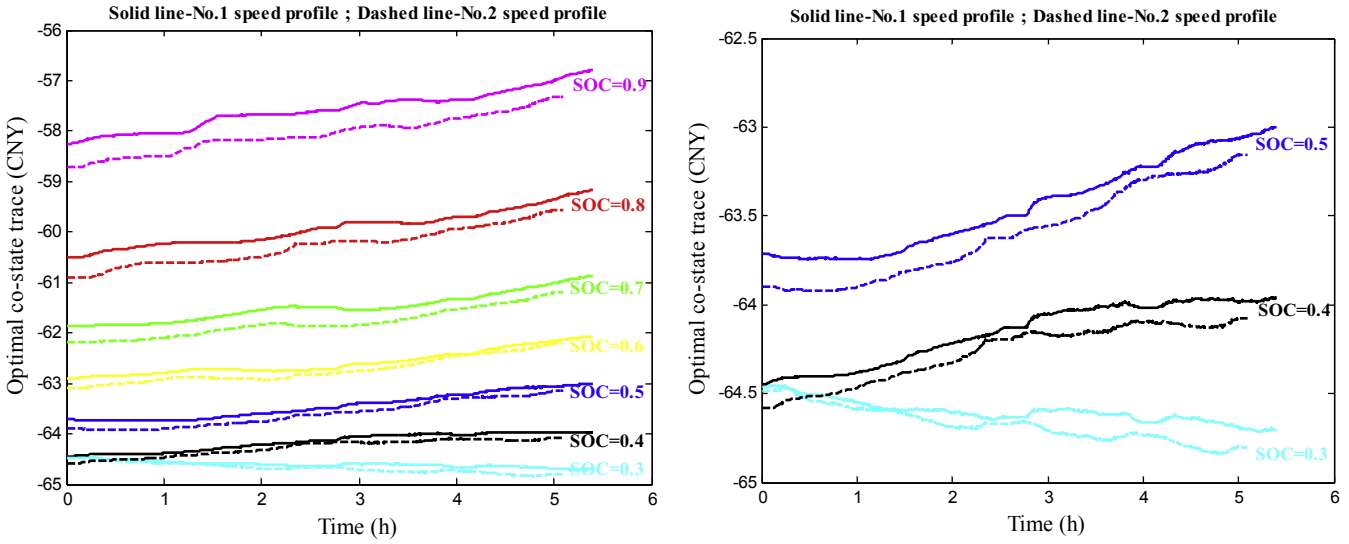

Fig. 11. (a) Optimal co-state traces for case 1 (two speed profiles). (b) Optimal co-state traces for case 1 (two speed profiles, initial SOC = 0.3, 0.4 and 0.5).

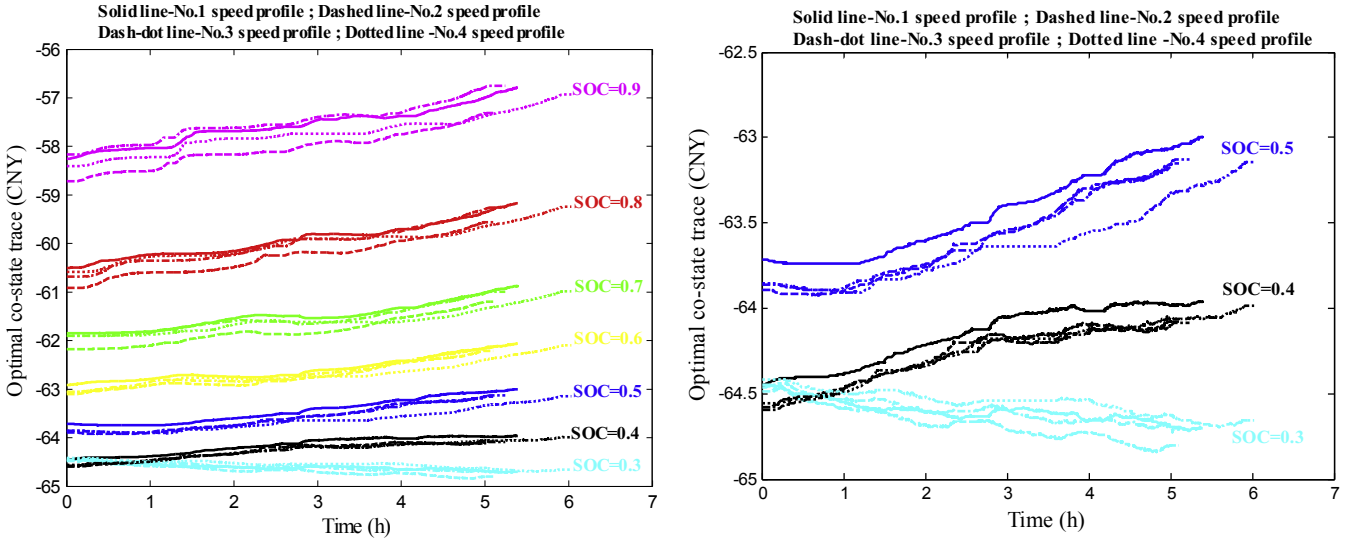

Fig. 12. (a) Optimal co-state traces for case 2 (four speed profiles). (b) Optimal co-state traces for case 2 (four speed profiles, initial SOC = 0.3, 0.4 and 0.5).

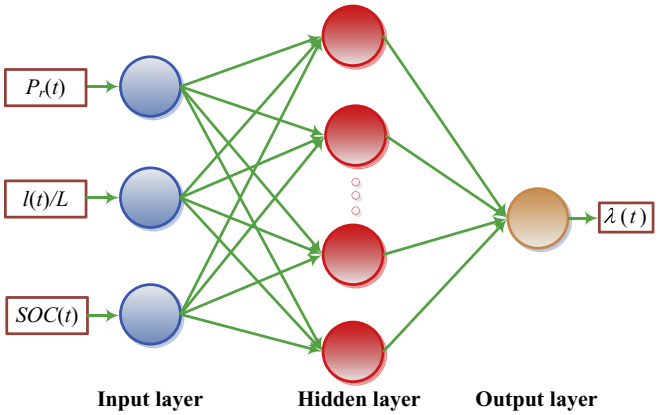

Fig. 13. Structure of artificial neural network.

time step, being set to 1s.

From Equation (15), it is evident that the demanded power depends on the speed at the current time step $v(k)$ and the previous one $v(k-1)$.

The total trip distance L is known for the city bus route, and the distance travelled l is determined by integrating the speed,

$$l = \sum_{i=1}^{t_n} v_i \Delta t \tag{16}$$

where t_n is the current time.

The network output is the co-state value, which reflects the power distribution between the battery and EGU.

Compared with existing neural network structures with many input variables [8,9,30], the proposed network with three inputs is simple but utilizes sufficiently varied information to determine the co-state. In fact, the selection of the three input variables is somewhat inspired by the SOC reference for the SOC feedback

based EMSs [17] or predictive EMSs [14].

5.2. Neural network training

As stated in Section 4.1, to evaluate the impact of sample size on the neural network performance, two neural networks are considered: ANN-2 (based on No.1 - No.2 speed profiles) and ANN-4 (based on No.1 - No. 4 speed profiles). Also, the specifications of the neural network applied to both networks are summarized in Table 2.

The main procedures of the neural network training are given as follows [35,36]:

Step 1: Neural network initialization.

Assume that n ($i = 1,2, \ldots,n$), q ($j = 1,2, \ldots q$) and m ($k = 1,2, \ldots,m$) denote the node numbers of the input, hidden, and output layers, respectively, and i, j, and k denote the i^{th}, j^{th}, and k^{th} neurons in the three layers, respectively. For this proposed ANN, it is known that $n = 3$, $q = 8$, and $m = 1$. Also, assume that ω_{ij} denotes the weights between the input and hidden layers, and ω_{jk} denotes the weights between the hidden and output layers.

Step 2: Compute the hidden layer.

$$G = f\left(\sum_{i=1}^{n} \omega_{ij} x_i - a_j\right) \tag{17}$$

where G is the output of the hidden layer, f is the activation function, x is the element of the input layer, and a is the threshold of the hidden layer.

Step 3: Compute the output layer.

With the hidden layer output G, the weights ω_{jk}, and the threshold of the output layer b_k, the predicted output of the neural network O_k can be computed as

$$O_k = \sum_{j=1}^{l} G_j \omega_{jk} - b_k. \tag{18}$$

Step 4: Compute the error and update the weights.

$$\begin{cases} e_k = Y_k - O_k \\ \omega_{ij} = \omega_{ij} + \eta G_j (1 - G_j) x_i \sum_{j=1}^{q} \omega_{jk} e_k \\ \omega_{jk} = \omega_{jk} + \eta G_j e_k \end{cases} \tag{19}$$

where e is the prediction error, and η is the learning ratio.

Step 5: Update the thresholds.

$$\begin{cases} a_j = a_j + \eta G_j (1 - G_j) x_i \sum_{k=1}^{m} \omega_{jk} e_k \\ b_k = b_k + e_k. \end{cases} \tag{20}$$

Table 2
Specifications of neural network.

Item	Value
Number of hidden layer nodes	8
Iterative time	100
Learning ratio	0.1
Learning target	0.00004
Activation function	$\frac{1}{1 - e^{-x}}$

6. ANN-ECMS

Fig. 14 outlines the framework of the proposed ANN-ECMS. The relationship between the EF (S) and the co-state variable (λ) is first established by comparing the PMP method and the ECMS, as described in Equation (13). Then, an artificial neural network is constructed, and the PMP method is applied to samples of speed profiles to acquire network training data. With the trained neural network, the optimal co-state can be determined online. Consequently, the optimal EF can be determined according to Equation (13), for use in the ECMS.

7. Results and discussion

Both the ANN-ECMS-2 (based on ANN-2) and ANN-ECMS-4 (based on ANN-4) are verified using the No. 5 speed profile with four initial SOCs (0.85, 0.65, 0.45, and 0.35). The outcomes of typical global optimization methods, including the DP and PMP algorithms, as well as the rule-based charging-depleting and charging-sustaining (CD-CS) strategy, are also presented in this section for comparisons. The discretization of the SOC for the DP method greatly affects the solution accuracy and the computational time. Thus, in order to make a fair comparison with other methods, the number of discrete SOC points is set to 400 after several trials. The prices of fuel and electricity are set at 5.4 CNY.L^{-1} and 0.8 CNY.kWh^{-1}, respectively. All simulations were performed in the Matlab environment on a laptop computer with a 2.3-GHz CPU and 8-GB memory.

The simulation results of these different methods considered are summarized in Table 3, which is divided into four blocks, highlighted by different colors, depending on the initial SOC.

From this Table, it is known that the total costs with high initial SOC levels are less than those with low levels, because higher initial SOCs allow inexpensive battery energy (electricity) to be used in greater proportions, resulting in smaller total costs. Comparing the results of the ANN-ECMS-2 and ANN-ECMS-4 methods within each block shows that they always have similar total costs, indicating that the performance of the ANN-ECMS is unaffected by an increase in the training sample size from 2 to 4 speed profiles. This could be due to the fact that the traffic environment along the city bus route remains relatively consistent over a half-year period, so that the two speed profiles are sufficient to reflect the traffic environment along the city bus route.

It can be seen that ANN-ECMSs deliver comparable fuel economy to that of the global optimization methods (DP and PMP) in all cases. Besides, the PMP always yields a lower total cost than the DP method, despite both being global optimization methods, because interpolating calculations needed by the DP algorithm to estimate the cost-to-go value affects the accuracy. As a rule-based strategy without any optimization, the CD-CS obviously leads to the lowest fuel economy.

Additionally, with initial SOCs of 0.65, 0.45, and 0.35, ANN-ECMSs have smaller total costs than do the PMP and DP methods. This is because the final SOCs of the ANN-ECMSs in these cases have fallen under the preset lower boundary value of 0.3, so the PHEV has consequently consumed a greater proportion of inexpensive battery energy, leading to slightly smaller total costs for the ANN-ECMSs, versus the other methods.

As for the computational time, Table 3 suggests that the CD-CS method always yields the smallest computational time, whereas the DP method is most time-consuming in all cases. Compared to the DP algorithm, the computational time of the PMP algorithm is greatly reduced. It can also be exposed that both ANN-ECMS-2 and ANN-ECMS-4 maintain a similar computational efficiency in all cases. Although the computational time of ANN-ECMSs is greater

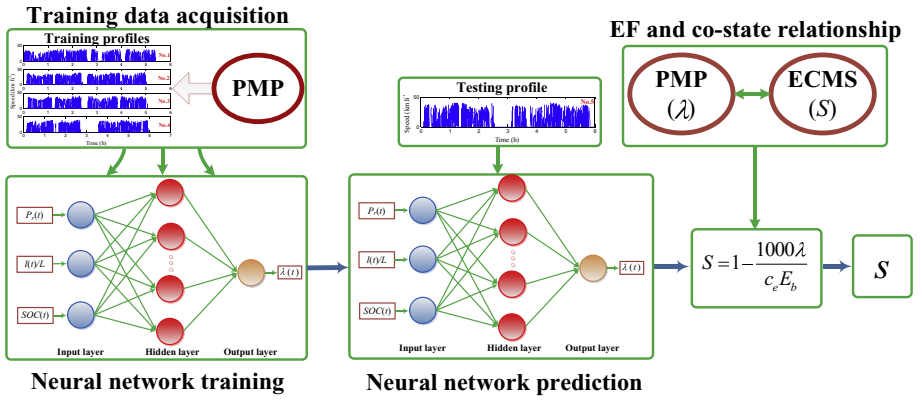

Fig. 14. Framework of ANN-ECMS.

Table 3
Simulation results of different methods.

Method	Initial SOC	F.C.(L)	E.C. (kWh)	Total cost (CNY)	Final SOC	Computation time (s)
DP	0.85	4.0862	53.9045	65.3114	0.3013	1361
PMP		3.9988	54.0951	64.9897	0.2994	57
ANN-ECMS-2		4.1462	53.5309	65.3386	0.3052	124
ANN-ECMS-4		4.0541	53.8799	65.1174	0.3016	125
CD-CS		7.2999	49.5495	79.2780	0.3475	8
DP	0.65	9.2508	34.1509	77.5524	0.3013	1359
PMP		9.1799	34.2961	77.2835	0.2999	56
ANN-ECMS-2		9.0440	34.8030	76.9513	0.2946	123
ANN-ECMS-4		9.0771	34.6772	77.0305	0.2959	124
CD-CS		14.5252	29.5155	102.4843	0.3500	8
DP	0.45	14.4890	14.5210	90.2920	0.3013	1360
PMP		14.4212	14.6496	90.0268	0.3000	31
ANN-ECMS-2		14.1499	15.6505	89.3543	0.2897	125
ANN-ECMS-4		14.2242	15.3736	89.5365	0.2926	129
CD-CS		21.6252	9.8330	125.2914	0.3500	9
DP	0.35	17.1256	4.7380	96.7825	0.3013	1362
PMP		17.0542	4.8562	96.4891	0.3001	38
ANN-ECMS-2		16.7418	6.0104	95.7163	0.2882	122
ANN-ECMS-4		16.8162	5.7340	95.8989	0.2911	120
CD-CS		25.0321	0.2821	136.1497	0.3475	9

Note: F.C. and E.C. stand for fuel consumption and electricity consumption respectively.

than that of the CD-CS method, its time efficiency, i.e., the computational time relative to the duration of the entire trip (6 h), suffices to ensure the development of a time-conscious EMS in real-time.

Figss. 15–18 depict the SOC profiles of different methods for the four cases considered. In Figs. 15–17, the SOC profiles of the DP, PMP, and both ANN-ECMSs exhibit a similar trend. In Fig. 18, the SOC profiles of the ANN-ECMSs slightly deviate from that of the PMP method. This can be explained by their different trends of SOC profiles. Specifically, the profiles with high initial SOC levels e.g. 0.9–0.4 decline approximately linearly and clearly feature slopes from an overall perspective, whereas the profiles with a low initial SOC level, e.g. 0.3, almost fluctuates around a horizontal line. Therefore, the case with an initial SOC of 0.35, close to the low

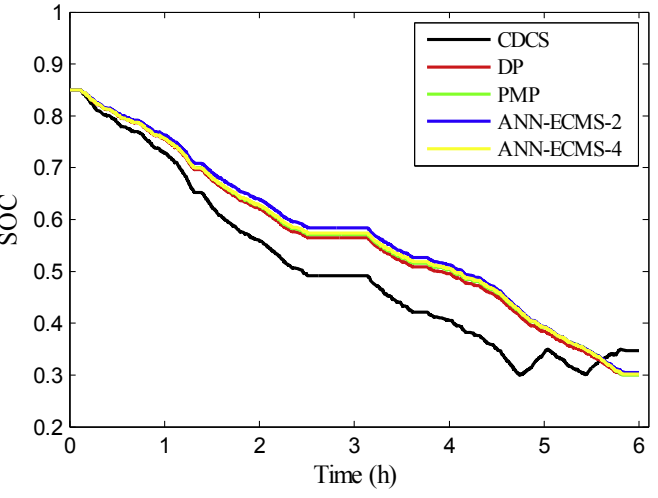

Fig. 15. SOC profiles of different methods (Initial SOC = 0.85).

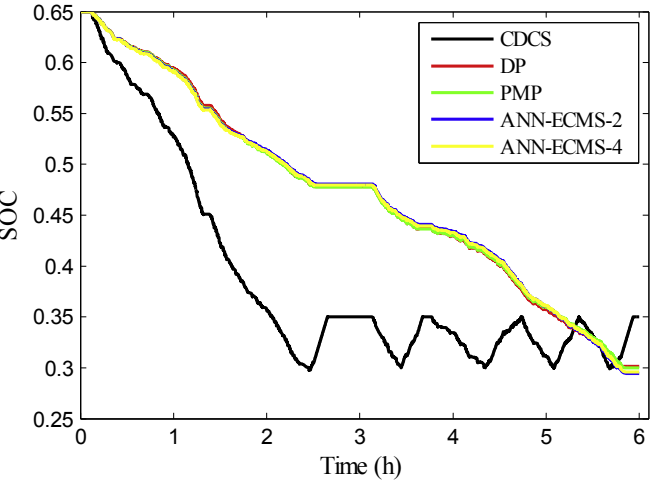

Fig. 16. SOC profiles of different methods (Initial SOC = 0.65).

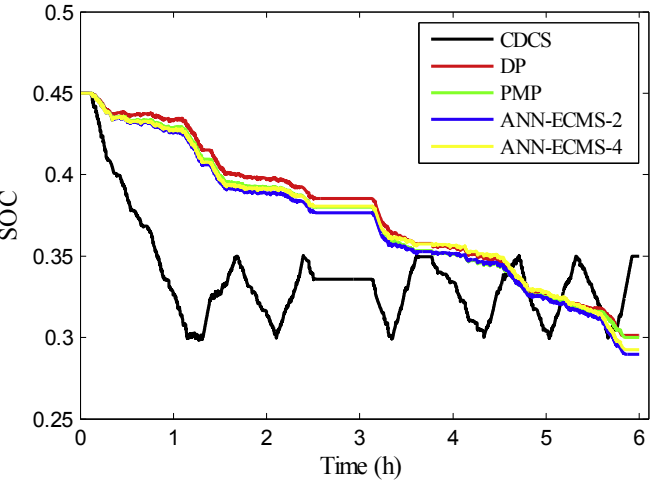

Fig. 17. SOC profiles of different methods (Initial SOC = 0.45).

nitial SOC level (0.3), is affected accordingly, leading to a slight difference from the SOC profile of the PMP method. However,

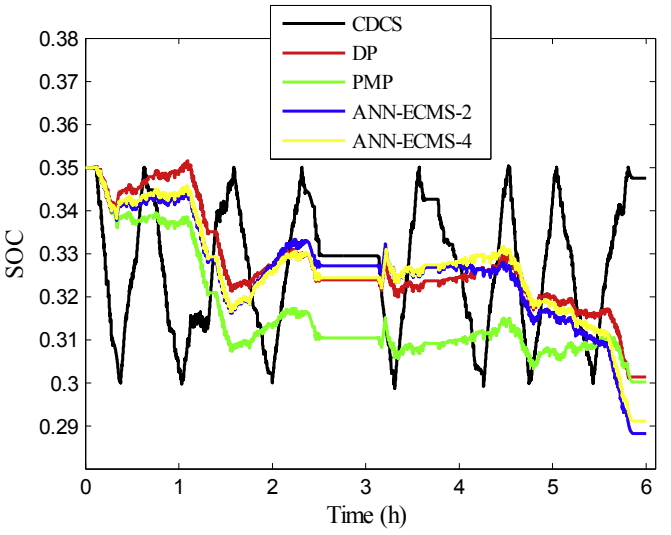

Fig. 18. SOC profiles of different methods (Initial SOC = 0.35).

overall, these SOC profiles are nearly overlapped, which induces virtually identical electricity energy consumption. The difference in the SOC profiles of the DP and PMP methods is mainly attributed to their different optimization mechanisms: the PMP algorithm determines the power allocation by minimizing the Hamiltonian function under SOC boundary constraints and other physical limitations, whereas the DP algorithm obtains the optimal solution by minimizing the cost-to-go value based on the Bellman Principle. With initial SOCs of 0.85, 0.65, and 0.45, the CD-CS strategy, with SOC thresholds for switching the EGU on/off being set to 0.35 and 0.30, respectively, first experiences a CD stage, followed by a CS stage. However, with an initial SOC of 0.35, the CS stage lasts throughout the trip.

To further demonstrate the solving process of the ANN-ECMS, Fig. 19 portrays the optimal co-state traces for the PMP method and the ANN-ECMSs in all cases. It is noticed that, at most times, the optimal co-state traces of the ANN-ECMSs approach the optimal co-state trace of the PMP method. However, in the final phase of the trip (roughly 4.8 h - 6 h), the traces experience a sharp change. This is because the optimal co-state traces with an initial SOC of 0.3 decline with time (see Figs. 11 (b) and Fig. 12 (b)), whereas those with initial SOC s of 0.4, 0.5, 0.6, 0.7, 0.8, and 0.9 rise with time. Therefore, a drop in optimal co-state values occurs when the SOC is in the proximity of 0.3 at the final portion of the trip. Accordingly, the EF traces of the ANN-ECMS-2 and ANN-ECMS-4 are illustrated in Fig. 20, based on the relationship expressed in Equation (13).

Furthermore, it can be unveiled in Fig. 19 that the discrepancies of the co-state traces between the ANN-ECMS and PMP with an initial SOC of 0.85 are more noticeable than those with an initial SOC of 0.65, 0.45, or, 0.35. ANN-ECMS-2 is taken as an example to explain such a phenomenon. In Fig. 11(a), as the initial SOC decreases from 0.9 to 0.3, the width between the co-state traces of No. 1 and No. 2 speed profiles (denoted as internal belt width) almost reduces, and the width between the neighboring two internal belts (denoted as external belt width) also reduces. When the initial SOC = 0.85, the ANN-ECMS-2 cannot accurately identify which co-state trace is better (co-state trace of No. 1 speed profile or No. 2 speed profile) or which group of co-state traces is better (group 1 - the co-state traces with an initial SOC of 0.9 or group 2 - the co-state traces with an initial SOC of 0.8), for the neural network to follow. As a result, the predicted co-state traces with an initial SOC of 0.85 are more fluctuating than those with an initial SOC of 0.65, 0.45, or

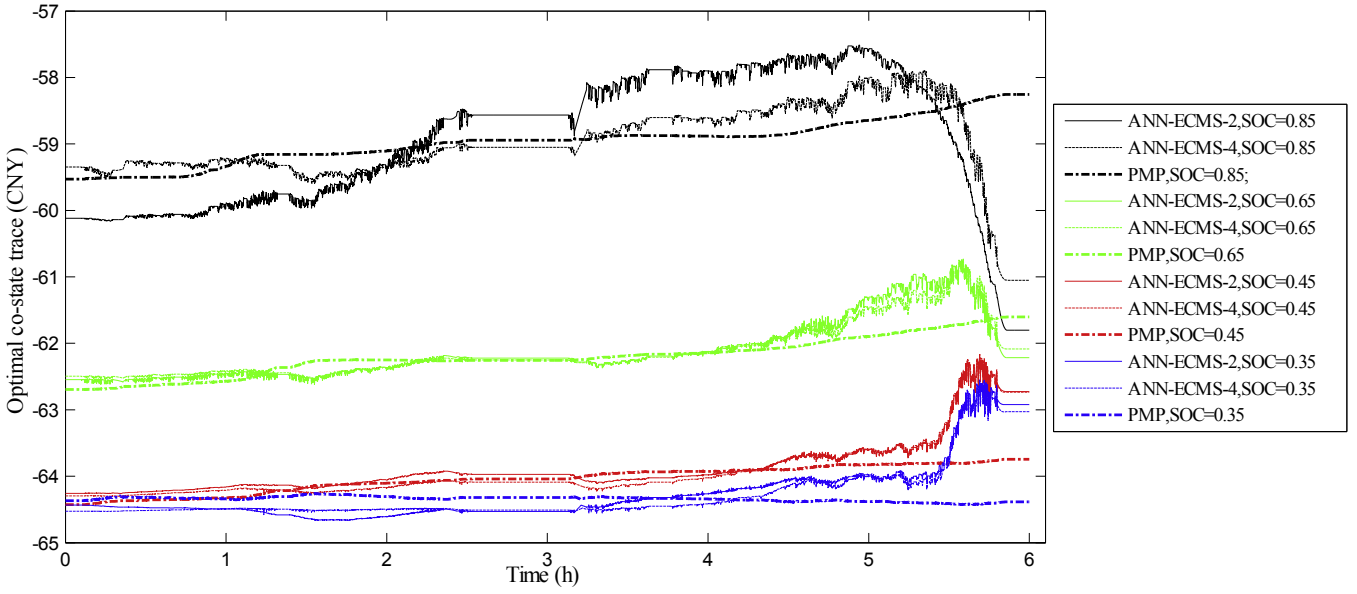

Fig. 19. Optimal co-state traces in all cases.

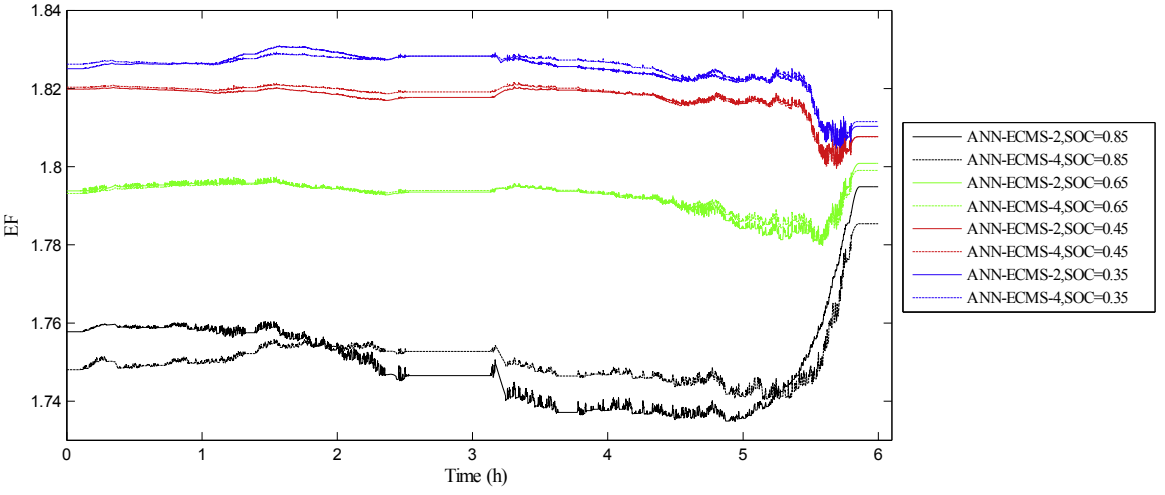

Fig. 20. EF traces in all cases.

0.35, and the associated discrepancies of the co-state traces between the ANN-ECMS and PMP look more obvious.

8. Conclusions

This paper proposes a data-driven energy management strategy for PHEVs, i.e., an artificial neural network improved equivalent consumption minimum strategy (ANN-ECMS). The ANN-ECMS dynamically identifies the equivalent factor (EF) for the ECMS using an artificial neural network. Three accessible input variables to the ANN, including the current demanded power, the ratio of the distance travelled to the total distance, and the battery SOC, are picked. Real-world speed profiles, along with the relationship between Pontryagin's Minimum Principle (PMP) and ECMS, are leveraged to train the neural network. Simulations considering various initial SOC levels are carried out. The results disclose that the proposed ANN-ECMS induces similar fuel economy to global optimization methods such as the DP and PMP methods, and significantly reduces the total energy consumption cost, compared to the rule-based charge-depleting and charge-sustaining (CD-CS) method, by 17.7%, 24.9%, 28.7%, and 29.6% for the initial SOC levels of 0.85, 0.65, 0.45, and 0.35, respectively. Furthermore, we can find that the performance of the ANN-ECMS is not significantly affected by an increase in the training sample size from 2 to 4 speed profiles for the case study of a city bus. In addition, the computational time of the ANN-ECMS indicates its great promise for the development of a time-efficient EMS for real-time vehicular applications.

As the city bus route considered in this paper is fixed with a largely consistent traffic environment, future studies could extend this method to passenger cars by mining trip/driving pattern statistics.

Acknowledgements

This work was supported in part by the EU-funded Marie Sklodowska-Curie Individual Fellowships (IF) Project under Grant

706253-pPHEV-H2020-MSCA-IF-2015, and in part by Fundamental Research Funds for Central Universities, China No.106112017CDJQJ338811 and No. 106112016CDJXZ338825).

References

[1] Martinez CM, Hu X, Cao D, Velenis E, Gao B, Wellers M. Energy management in plug-in hybrid electric vehicles: recent progress and a connected vehicles perspective. IEEE Trans Veh Technol 2017;66(6):4534–49.

[2] Hu X, Zou Y, Yang Y. Greener plug-in hybrid electric vehicles incorporating renewable energy and rapid system optimization. Energy 2016;111:971–80.

[3] Yang C, Jiao X, Li L, Zhang Y, Zhang L, Song J. Robust coordinated control for hybrid electric bus with single-shaft parallel hybrid powertrain. IET Control Theory & Appl 2014;9(2):270–82.

[4] Schouten NJ, Salman MA, Kheir NA. Fuzzy logic control for parallel hybrid vehicles. IEEE Trans Contr Syst Technol 2002;10(3):460–8.

[5] Sciarretta A, Back M, Guzzella L. Optimal control of parallel hybrid electric vehicles. IEEE Trans Contr Syst Technol 2004;12(3):352–63.

[6] Serrao L, Onori S, Rizzoni G. ECMS as a realization of Pontryagin's minimum principle for HEV control. In: Proc. Amer. Control conf. (ACC); 2009. p. 3964–9.

[7] Li L, Yang C, Zhang Y, Song J. Correctional DP-based energy management strategy of plug-in hybrid electric bus for city-bus route. IEEE Trans Veh Technol 2015;64(7):2792–803.

[8] Murphey YL, Park J, Kiliaris L, Kuang ML, Masrur MA, Phillips AM, Wang Q. Intelligent hybrid vehicle power control - part II: online intelligent energy management. IEEE Trans Veh Technol 2013;62(1):69–79.

[9] Chen Z, Mi CC, Xu J, Gong X, You C. Energy management for a power-split plug-in hybrid electric vehicle based on dynamic programming and neural networks. IEEE Trans Veh Technol 2014;63(4):1567–80.

[10] Yu H, Tarsitano D, Hu X, Cheli F. Real time energy management strategy for a fast charging electric urban bus powered by hybrid energy storage system. Energy 2016;112:322–31.

[11] Lin CC, Peng H, Grizzle JW, Kang JM. Power management strategy for a parallel hybrid electric truck. IEEE Trans Contr Syst Technol 2013;11(6):839–49.

[12] Johannesson L, Asbogard M, Egardt B. Assessing the potential of predictive control for hybrid vehicle powertrains using stochastic dynamic programming. IEEE Trans Intell Transport Syst 2007;8(1):71–83.

[13] Moura SJ, Fathy HK, Callaway DS, Stein JL. A stochastic optimal control approach for power management in plug-in hybrid electric vehicles. IEEE Trans Contr Syst Technol 2011;19(3):545–55.

[14] Xie S, Hu X, Xin Z, Li L. Time-efficient stochastic model predictive energy management for a plug-in hybrid electric bus with adaptive reference state-of-charge advisory. IEEE Trans Veh Technol 2018;67(7):5671–82.

[15] Kim N, Cha S, Peng H. Optimal control of hybrid electric vehicles based on Pontryagin's minimum principle. IEEE Trans Contr Syst Technol 2011;19(5):1279–87.

[16] Onori S, Tribioli L. Adaptive Pontryagin's Minimum Principle supervisory controller design for the plug-in hybrid GM Chevrolet Volt. Appl Energy 2015;147:224–34.

[17] Xie S, Li H, Xin Z, Liu T, Wei LA. Pontryagin minimum principle-based adaptive equivalent consumption minimum strategy for a plug-in hybrid electric bus on a fixed route. Energies 2017;10(9):1379–99.

[18] Yang C, Li L, You S, Yan B, Du X. Cloud computing-based energy optimization control framework for plug-in hybrid electric bus. Energy 2017;125:11–26.

[19] Unger J, Kozek M, Jakubek S. Nonlinear model predictive energy management controller with load and cycle prediction for non-road HEV. Contr Eng Pract 2015;36:120–32.

[20] Musardo C, Rizzoni G, Guezennec Y, Staccia B. A-ECMS: an adaptive algorithm for hybrid electric vehicle energy management. Eur J Contr 2005;11(4):509–24.

[21] Tulpule P, Marano V, Rizzoni G. Energy management for plug-in hybrid electric vehicles using equivalent consumption minimization strategy. Int J Electric and Hybrid Veh 2010;2(4):329–50.

[22] Sivertsson M, Eriksson L. Design and evaluation of energy management using map-based ECMS for the PHEV benchmark. Oil Gas Sci Technol 2015;70(1):195–211.

[23] Onori S, Serrao L. On Adaptive-ECMS strategies for hybrid electric vehicles. In: Proceedings of the international scientific conference on hybrid and electric vehicles; 2011. p. 6–7.

[24] Sivertsson M, Eriksson L. Design and evaluation of energy management using map-based ECMS for the PHEV benchmark. Oil Gas Sci Technol 2015;70(1):195–211.

[25] Feng T, Yang L, Gu Q, Hu Y, Yan T, Yan B. A supervisory control strategy for plug-in hybrid electric vehicles based on energy demand prediction and route preview. IEEE Trans Veh Technol 2015;64(5):1691–700.

[26] Sun C, Sun F, He H. Investigating adaptive-ECMS with velocity forecast ability for hybrid electric vehicles. Appl Energy 2017;185:1644–53.

[27] Zhang Y, Chu L, Fu Z, Xu N, Guo C, Zhang X, Wang P. Optimal energy management strategy for parallel plug-in hybrid electric vehicle based on driving behavior analysis and real time traffic information prediction. Mechatronics 2017;46:177–92.

[28] Yang C, Du S, Li L, You S, Yang Y, Zhao Y. Adaptive real-time optimal energy management strategy based on equivalent factors optimization for plug-in hybrid electric vehicle. Appl Energy 2017;203:883–96.

[29] Zhang F, Liu H, Hu Y, Xi J. A supervisory control algorithm of hybrid electric vehicle based on adaptive equivalent consumption minimization strategy with fuzzy PI. Energies 2016;9:919.

[30] Tian H, Li SE, Wang X, Huang Y, Tian G. Data-driven hierarchical control for online energy management of plug-in hybrid electric city bus. Energy 2018;142:55–67.

[31] Wang J, Xie S, Liu X, Yuan Y, Li B, Li S, et al. Research and development of a chassis for the extended-range and plug-in commercial vehicle. Shaanxi automobile Group Research Report. 2015 [In Chinese].

[32] Johnson VH. Battery performance models in ADVISOR. J Power Sources 2002;110(2):321–9.

[33] Paganelli G, Delprat S, Guerra TM, Rimaux J, Santin JJ. Equivalent consumption minimization strategy for parallel hybrid powertrains. Vehicular Technology Conference, 2002. VTC Spring 2002. In: IEEE 55th. IEEE, vol. 4; 2002. p. 2076–81.

[34] Serrao L, Onori S, Rizzoni G. A comparative analysis of energy management strategies for hybrid electric vehicles. J Dyn Syst Meas Contr 2011;133(3):031012.

[35] Wang X, Shi F, Yu L, Li Y. Case study of Matlab neural network. Beijing: Beihang University Press; 2016 [In Chinese)].

[36] Haykin S. Neural networks: a comprehensive foundation. US: Pearson Education Press; 1997.